Received: 30 April 2021 | Revised: 23 June 2021 | Accepted: 27 June 2021

DOI: 10.1002/hyp.14296

RESEARCH ARTICLE

WILEY

# Estimating flow resistance in steep slope rills

Costanza Di Stefano[1] | Alessio Nicosia[1] | Vincenzo Palmeri[1] | Vincenzo Pampalone[1] | Vito Ferro[2]

[1]Department of Agricultural, Food and Forest Sciences, University of Palermo, Palermo, Italy

[2]Department of Earth and Marine Science, University of Palermo, Palermo, Italy

**Correspondence**
Vincenzo Pampalone, Department of Agricultural, Food and Forest Sciences, University of Palermo, Viale delle Scienze, Building 4, 90128, Palermo, Italy.
Email: vincenzo.pampalone@unipa.it

## Abstract

Recent research recognized that the slope of 18% can be used to distinguish between the 'gentle slope' case and that of 'steep slope' for the detected differences in hydraulic variables (flow depth, velocity, Reynolds number, Froude number) and those representatives of sediment transport (flow transport capacity, actual sediment load). In this paper, using previous measurements carried out in mobile bed rills and flume experiments characterized by steep slopes (i.e., slope greater than or equal to 18%), a theoretical rill flow resistance equation to estimate the Darcy-Weisbach friction factor is tested. The main aim is to deduce a relationship between the velocity profile parameter $\Gamma$, the channel slope, the Reynolds number, the Froude number and the textural classes using a data base characterized by a wide range of hydraulic conditions, plot or flume slope (18%–84%) and textural classes (clay ranging from 3% to 71%). The obtained relationship is also tested using 47 experimental runs carried out in the present investigation with mobile bed rills incised in a 18%—sloping plot with a clay loam soil and literature data. The analysis demonstrated that: (1) the soil texture affects the estimate of the $\Gamma$ parameter and the theoretical flow resistance law (Equation 25), (2) the proposed Equation (25) fits well the independent measurements of the testing data base, (3) the estimate of the Darcy-Weisbach friction factor is affected by the soil particle detachability and transportability and (4) the Darcy-Weisbach friction factor is linearly related to the rill slope.

**KEYWORDS**
flow resistance, plot measurements, rill hydraulics, soil erosion, soil texture, steep hillslopes

## 1 | INTRODUCTION

Soil erosion is an important environmental problem around the world because it causes a large amount of soil loss (Bennett et al., 2015; Borrelli et al., 2017), non-point pollution (Wang et al., 2019), soil organic carbon loss and biodiversity reduction. Soil loss due to water erosion is a natural phenomenon and its acceleration, due to anthropogenic perturbations, can become intolerable for its on-farm and off-farm impacts (Bagarello et al., 2015; Di Stefano & Ferro, 2016).

Rill erosion, which is one mechanism of soil loss by water on hillslopes, is due to the detachment and transport of soil particles by channelized flows. Formation of rills occurs when surface flow gradually converts into concentrated flow, thereby leading to increased sediment yield with increasing flow shear stress and velocity. Rills are actively eroded channels, evolve morphologically over a short timescale and represent the main sediment source of eroded particles from hillslopes (Mutchler & Young, 1975; Zhang et al., 2016). The development of a rill network assures the transport of soil particles

both detached by rill flow and delivered from the interrill areas to the rill channels (Bagarello et al., 2015; Bagarello & Ferro, 2004, 2010; Bruno et al., 2008; Di Stefano et al., 2013; Di Stefano et al., 2015; Govers et al., 2007; Peng et al., 2015). Modelling of rill flow is necessary for an adequate simulation of rill erosion (Abrahams et al., 1996) and accurate rill measurements at plot scale allow both to understand the physical process and model rill erosion correctly (Wirtz et al., 2010, 2012). Rill erosion strictly depends on hydraulic characteristics of the flow moving within the rill (Foster et al., 1984) and for this reason to study and model rill erosion processes, in addition to flow discharge, other hydraulic variables as surface width, water depth, mean flow velocity and roughness coefficient must be defined (Gilley et al., 1990).

A rill is the print resulting from changes in width, depth and bed roughness due to the interaction between the erodible wetted perimeter of the channel and the flow. The rill morphology and the development of channelized erosion processes are affected by detached bed material and actual sediment transport occurring within a rill (Wang et al., 2015).

Rills are small, steep sloping (Nearing et al., 1997; Peng et al., 2015) and ephemeral channels in which shallow flows move. Therefore, rill hydraulics should be governed by physical laws quite different from those of open channel flows (Foster et al., 1984) which are characterized by a water depth much higher than the roughness representative size and a slower morphological evolution than rills. Govers et al. (2007) highlighted that equations obtained for alluvial rivers continue to be applied, while specific relationships for rill hydraulics are available (Abrahams et al., 1996; Di Stefano, Ferro, Palmeri, & Pampalone, 2017c; Foster et al., 1984; Gilley et al., 1990; Govers, 1992a; Hessel et al., 2003; Line & Meyer, 1988; Takken et al., 1998). Neglecting the actual difference between rills and rivers, classical hydraulic equations developed for fixed bed channels, such as Manning's and Chezy's equations, have been often used in physically based soil erosion models (Ferro, 1999; Govers et al., 2007; Nouwakpo et al., 2016; Powell, 2014; Strohmeier et al., 2014). In principle, the interaction among rill flow velocity, erosion of the rill wetted perimeter and sediment transport within the rill could hinder the applicability of the uniform open channel flow equations (Di Stefano et al., 2018a; Nearing et al., 1997).

Many authors (Peng et al., 2015; Stroosnijder, 2005; Wirtz et al., 2012) recognized that rill flow experiments can be useful both to overcome the scientific gap in rill hydraulics and to test the applicability of concepts and equations which are currently used in soil erosion modelling (Govers et al., 2007; Wirtz et al., 2010, 2012, 2013).

When a theoretical distribution can be applied to the velocity profiles measured in different verticals of the cross section (Ferro & Baiamonte, 1994), and the relationships that establish how the coefficients of the theoretical velocity profile distribution (Baiamonte et al., 1995; Ferro, 2003) vary from one vertical to another can be established, the flow resistance law can be theoretically obtained by an integration procedure.

The recurring unavailability of measured velocity distribution in different verticals of a cross-section and the complexity of the integration procedure justify the use of the following empirical flow resistance equations (Ferro, 1999; Powell, 2014):

$$V = C\sqrt{Rs} = \frac{s^{1/2}R^{2/3}}{n} = \sqrt{\frac{8gRs}{f}}, \quad (1)$$

in which $V$ (m s$^{-1}$) is the cross-section average velocity, $C$ (m$^{1/2}$ s$^{-1}$) is the Chezy coefficient, $n$ (m$^{-1/3}$ s) is the Manning coefficient, $f$ is the Darcy – Weisbach friction factor, $s$ is the channel slope, $R$ (m) is the hydraulic radius (m) and $g$ (m s$^{-2}$) is the acceleration due to gravity.

Most field and laboratory studies on overland and rill flow use the Darcy-Weisbach friction factor, whilst the use of Manning's $n$ is widespread in open channel flows (Hessel et al., 2003). However, this differentiation is not well-defined because "*Manning's n is likely to behave in the same way as f*" (Hessel et al., 2003; Takken & Govers, 2000). The Darcy-Weisbach friction factor is, as an example, currently used in WEPP (Water Erosion Prediction Project) (Foster et al., 1995; Govers et al., 2007; Nicosia et al., 2019).

Slope affects considerably the flow transport capacity $T_c$ (Ali et al., 2011; Ferro, 1998), which in turn influences the actual sediment transport. According to Jiang et al. (2018), the hydraulic mechanisms of soil erosion for steep slopes are different from those for gentle slopes. Recent experimental research on transport capacity for slopes steeper than 17%–18% (Ali et al., 2013; Wu et al., 2016; Zhang et al., 2009) established that $T_c$ relationships developed for gentle slopes (<18%) are unsuitable to be applied for steep slopes (17%–47%). Also, Peng et al. (2015) noticed that "*there has been little research concerning rill flow on steep slopes (e.g., slope gradients higher than 10°)*". For slope values greater than or equal to 18%, the measurements by Peng et al. (2015) showed that the flow is supercritical ($1.09 \le F \le 2.33$, where $F = V/(gh)^{0.5}$ is the Froude number of the flow and $h$ (m) is the water depth) with a flow regime varying from transitional to turbulent ($1140 \le Re \le 7629$, where $Re = Vh/\nu_k$ is the Reynolds number and $\nu_k$ (m$^2$ s$^{-1}$) is the water kinematic viscosity). On slopes less than 18% Peng et al. (2015) established that the friction factor decreases gradually as $Re$ increases, while on steeper slopes (21%–27%) $f$ increases gradually with the flow Reynolds number. According to these authors, these different *f-Re* trends indicate that slope gradient plays a fundamental role in determining roughness in rills. Peng et al. (2015) also suggested that, when $Re$ increases, on gentle slopes the effect of roughness reduction due to the flow depth increase is greater than that of roughness increase caused by sediment load and rill morphology. On the contrary, on steep slopes, this last effect, due to the intensified channelized erosion, prevails over the relative roughness reduction.

The slope of 18% could be used to distinguish between the "gentle slope' case from that of 'steep slope' for the possible difference in hydraulic (flow depth, velocity, Reynolds number, Froude number) and sediment transport variables (flow transport capacity, actual sediment load).

How the simultaneous increase of roughness and slope gradient affects flow resistance in a mobile bed rill continues to be a scientific

debated topic (Di Stefano, Ferro, Palmeri, & Pampalone, 2017c; Foster et al., 1984; Giménez & Govers, 2001; Govers, 1992a; Nearing et al., 1997; Torri et al., 2012). Govers (1992a) proposed a 'feedback mechanism' in which the expected increase of flow velocity with slope gradient is counterbalanced by a simultaneous increase of bed roughness, due to the increase of erosion rate with slope (Torri et al., 2012; Xinlan et al., 2015). The result of this 'feedback mechanism' is that, in a mobile bed rill, the flow velocity tends to be independent of slope (Nearing et al., 1997, 1999; Takken et al., 1998). According to Equation (1) the feedback mechanism can occur only if the Darcy-Weisbach friction factor $f$ increases linearly with slope gradient. The feedback mechanism does not occur in fixed bed rills, for which experiments by Foster et al. (1984) demonstrated that flow velocity increases with slope as roughness is slope-invariant.

Soil surface roughness is the key variable synthesizing the effects of soil surface irregularities due to soil particle size, rock fragments, vegetation cover and land management (Thomsen et al., 2015; Zhang et al., 2016). Grain resistance acting along the rill wetted perimeter is affected by soil particle and aggregate sizes. Recent improvements of survey technology by micro-topography techniques (Di Stefano, Ferro, Palmeri, Pampalone, & Agnello, 2017; Frankl et al., 2015; Gómez-Gutiérrez et al., 2014; James & Robson, 2012; Micheletti et al., 2015; Westoby et al., 2012) stimulated experiments finalized to a quantitative characterization of grain roughness and rill bed morphology (Carollo et al., 2015; Di Stefano, Ferro, Palmeri, & Pampalone, 2017b; Zhang et al., 2016).

In previous papers (Carollo et al., 2021; Di Stefano et al., 2018a; Di Stefano, Ferro, Palmeri, & Pampalone, 2017c; Di Stefano, Nicosia, Palmeri, et al., 2019; Di Stefano, Nicosia, Pampalone, et al., 2019; Palmeri et al., 2018), the Π-Theorem of the dimensional analysis and the self-similarity theory (Barenblatt, 1979, 1987) allowed to deduce a theoretical rill flow resistance equation based on the integration of a power velocity distribution. The applicability of this theoretical flow resistance equation was tested by measurements carried out in rills (Di Stefano et al., 2018a; Di Stefano, Ferro, Palmeri, & Pampalone, 2017c; Palmeri et al., 2018), shaped on experimental plots having different slope values $s_p$ (9%, 14%, 22%, 24% and 26%) and soil textures, joined with literature data (Jiang et al., 2018; Peng et al., 2015; Strohmeier et al., 2014).

Previous experiments (Jiang et al., 2018; Peng et al., 2015) induce to consider that additional work must be done on hydraulics of rills on steep slopes (i.e., slope gradient greater than or equal to 18%). In this paper, using experimental measurements carried out in recent studies (Di Stefano et al., 2018a; Di Stefano, Nicosia, Palmeri, et al., 2019; Huang et al., 2020; Jiang et al., 2018; Palmeri et al., 2018; Yang et al., 2020) the applicability of the theoretical rill flow resistance equation is further tested for the steep slope condition. In particular, the data base constituted by rill (Di Stefano et al., 2018a; Di Stefano, Nicosia, Palmeri, et al., 2019; Palmeri et al., 2018) and flume measurements (Huang et al., 2020; Jiang et al., 2018) carried out for steep slopes (Table 1), is used to calibrate a relationship for estimating the velocity profile parameter Γ. Then the reliability of the latter and the theoretical rill flow resistance equation are verified using independent measurements carried out in this investigation and by Yang et al. (2020).

## 2 | DEDUCING VELOCITY PROFILE AND RILL FLOW RESISTANCE LAW

For an open channel flow the local flow velocity distribution $v(y)$ along a given vertical is expressed by the following functional relationship (Barenblatt, 1987, 1993; Di Stefano, Ferro, Palmeri, & Pampalone, 2017c; Ferro, 1997):

$$\phi\left(\frac{dv}{dy}, y, h, d, u_*, s, \varrho, \mu, g\right) = 0, \tag{2}$$

in which $\phi$ is a functional symbol, $y$ is the distance from the bottom, $h$ is water depth, $d$ is a characteristic diameter, $u_* = \sqrt{g\,R\,s}$ is the shear velocity, $\rho$ is the water density and $\mu$ is the dynamic water viscosity.

Using as dimensional independent variables $y$, $u_*$ and $\mu$, and applying the Π-Theorem of the dimensional analysis the following dimensionless groups are obtained:

$$\Pi_1 = \frac{y}{u_*}\frac{dv}{dy}, \tag{3}$$

**TABLE 1** Slope and textural characteristics of the available database

| | Calibrating data set | | | | | | | Testing data set | |
|---|---|---|---|---|---|---|---|---|---|
| Authors | Di Stefano et al. (2018a) | Palmeri et al. (2018) | | Di Stefano, Nicosia, Palmeri, et al. (2019) | | Jiang et al. (2018) | Huang et al. (2020) | Yang et al. (2020) | This investigation |
| slope $s_p$ (%) | 22 | 24 | 26 | 18 | 25 | 18, 27, 36, 47, 58, 70, 84 | 17.6, 26.8, 36.4 | 17.6, 26.8, 36.4, 46.6 | 18 |
| clay (%) | 62 | 42 | 71 | 62 | 71 | 3 | 11.6 | 25.9 | 32.7 |
| silt (%) | 26.4 | 23.5 | 19.9 | 26.4 | 19.9 | 32.8 | 64.6 | 69.8 | 30.9 |
| sand (%) | 11.6 | 34.5 | 9.1 | 11.6 | 9.1 | 64.2 | 23.8 | 4.3 | 36.4 |

*Note:* $s_p$, plot or flume slope; clay, clay fraction of the investigated soil; silt, silt fraction of the investigated soil; sand, sand fraction of the investigated soil.

$$\Pi_2 = \frac{h}{y}, \tag{4}$$

$$\Pi_3 = \frac{d}{y}, \tag{5}$$

$$\Pi_4 = s, \tag{6}$$

$$\Pi_5 = \frac{u_* y}{\nu_k}, \tag{7}$$

$$\Pi_6 = \frac{g y}{u_*^2}. \tag{8}$$

Barenblatt (1987) also underlined that "*In some cases, it turns out to be convenient to choose new similarity parameters – products of powers of the similarity parameters obtained in the previous step*". In other words, Barenblatt (1987) suggested to combine the original dimensionless groups to obtain new similarity parameters $\Pi_i$.

From Equations (4) and (5) it follows:

$$\Pi_{2,3} = \frac{\Pi_2}{\Pi_3} = \frac{h}{d}. \tag{9}$$

Coupling Equations (7), (5) and (9) the following equation is obtained:

$$\Pi_{5,3,2} = \sqrt{\frac{8}{f}}\Pi_5 \Pi_3 \Pi_2 = \frac{V h}{\nu_k} = Re, \tag{10}$$

while from Equations (8) and (4) it follows

$$\Pi_{6,2} = \sqrt{\frac{8}{f}}\frac{1}{\Pi_6^{1/2}\Pi_2^{1/2}} = \frac{V}{\sqrt{g h}} = F. \tag{11}$$

The functional relationship (2) can be rewritten in the following form:

$$\Pi_1 = \phi_1(\Pi_{2,3}, \Pi_4, \Pi_5, \Pi_{5,3,2}, \Pi_{6,2}), \tag{12}$$

where $\phi_1$ is a functional symbol.

Introducing into Equation (12) the expression of each dimensionless group, the functional relationship can be rewritten as follows:

$$\frac{y}{u_*}\frac{dv}{dy} = \phi_2\left(\frac{h}{d}, s, \frac{u_* y}{\nu_k}, Re, F\right), \tag{13}$$

where $\phi_2$ is a functional symbol.

Assuming the Incomplete Self-Similarity (ISS) in $u \cdot y/\nu_k$ (Barenblatt & Monin, 1979; Barenblatt & Prostokishin, 1993; Butera et al., 1993; Ferro, 2017; Ferro & Pecoraro, 2000), Equation (13) yields:

$$\frac{1}{u_*}\frac{dv}{dy} = \left(\frac{1}{y}\frac{u_* y}{\nu_k}\frac{\nu_k}{u_* y}\right)\left(\frac{u_* y}{\nu_k}\right)^{\delta}\phi_3\left(\frac{h}{d}, s, Re, F\right), \tag{14}$$

in which $\phi_3$ is a functional symbol and $\delta$ is a coefficient.

Rearranging Equation (14) results in

$$\frac{1}{u_*}\frac{dv}{dy} = \left(\frac{u_*}{\nu_k}\right)\left(\frac{u_* y}{\nu_k}\right)^{\delta-1}\phi_4\left(\frac{h}{d}, s, Re, F\right), \tag{15}$$

where $\phi_4$ is a functional symbol.

According to Ferro (2018), the flow Froude number takes also into account the ratio $h/d$ and integrating Equation (15) the following power velocity distribution is obtained:

$$\frac{v}{u_*} = \left[\frac{1}{\delta}\phi_4(s, Re, F)\right]\left(\frac{u_* y}{\nu_k}\right)^{\delta} + C_i, \tag{16}$$

in which $C_i$ is integration constant. According to experimental results (Barenblatt & Prostokishin, 1993; Butera et al., 1993; Ferro & Pecoraro, 2000) the integration constant $C_i$ can be assumed equal to zero and Equation (16) can be rewritten as follows:

$$\frac{v}{u_*} = \Gamma(s, Re, F)\left(\frac{u_* y}{\nu_k}\right)^{\delta}, \tag{17}$$

in which $\Gamma(s, Re, F)$ is a function of channel slope, Reynolds number and flow Froude number to be defined by velocity measurements and the exponent $\delta$ can be calculated by the following theoretical equation (Barenblatt, 1991; Castaing et al., 1990)

$$\delta = \frac{1.5}{\ln Re}. \tag{18}$$

Integrating the velocity distribution (Equation 17), the following expression of the Darcy-Weisbach friction factor $f$ is deduced (Barenblatt, 1993; Ferro, 2017; Ferro & Porto, 2018):

$$f = 8\left[\frac{2^{1-\delta}\Gamma Re^{\delta}}{(\delta+1)(\delta+2)}\right]^{-2/(1+\delta)}. \tag{19}$$

From Equation (17) the following estimate $\Gamma_v$ of $\Gamma$ function (Ferro, 2017; Ferro & Porto, 2018) can be obtained by setting $y = \alpha h$, being $\alpha h$ the distance from the bottom at which the local velocity is equal to the cross-section average velocity $V$:

$$\Gamma_v = \frac{V}{u_*\left(\frac{u_* \alpha h}{\nu_k}\right)^{\delta}}. \tag{20}$$

The coefficient $\alpha$ is less than 1 and takes into account that: (a) the average velocity $V$ is located below the water surface and, (b) the mean velocity profile in the cross-section is considered (i.e., the velocity profile is obtained by averaging for each $y$ the $v$ values measured in different verticals, and its integration gives the cross-section average velocity). The coefficient $\alpha$ has to be calculated by the following theoretical relationship deduced by Ferro (2017):

$$\alpha = \left[\frac{2^{1-\delta}}{(\delta+1)(\delta+2)}\right]^{1/\delta}. \quad (21)$$

Considering that, according to Equation (17), $\Gamma$ theoretically depends only on channel slope, Reynolds number and flow Froude number (Ferro, 2018), $\Gamma_v$ can be estimated by $s$, $Re$ and $F$ using the following power equation:

$$\Gamma_v = a\frac{F^b}{s^c Re^e}, \quad (22)$$

where $a$, which summarizes the effect of the soil characteristics on the flow resistance law, $b$, $c$ and $e$ are coefficients to be determined from experimental measurements.

For considering the effect of soil texture (Carollo et al., 2021), the following equation to estimate the scale factor $\Gamma_v$ of the velocity profile can be applied:

$$\Gamma_v = \left(\frac{a_o \mathrm{CLAY}^m}{\mathrm{SILT}^p}\right)\frac{F^b}{s^c Re^e}, \quad (23)$$

in which $a_o$, $m$ and $p$ are coefficients to be determined by measurements carried out in rills incised in soils having different texture and CLAY and SILT are the percentage of clay and silt of the investigated soil, respectively. In Equation (23) the soil texture effects on rill flow resistance are modelled by clay and silt percentages which represent the influence of the detachability and transportability properties of the soil particles. Reynolds number was introduced into Equation (23) for considering that (i) the velocity distribution is affected by flow regime and (ii) the range of the experimental $Re$ values used to calibrate this equation could be wide and involving different flow regimes.

## 3 | MATERIALS AND METHODS

### 3.1 | Experiments by Di Stefano et al. (2018a); Di Stefano, Nicosia, Palmeri, et al. (2019) and Palmeri et al. (2018)

Two plots, located at the experimental area of the Department of Agriculture, Food and Forest Sciences of the University of Palermo, were used to carry out these experiments. Each plot was 2 m wide and 7 m long. Table 1 reports the textural fractions, and the plot slope values $s_p$ of this data base, which is characterized by clay fractions ranging from 42% to 71%, silt of 19.9%–26.4%, sand in the range 9.1% – 34.5% and slope values $s_p$ varying from 18% to 26%. The experiments were carried out using a constant inflow discharge ranging from 0.11 to 1 L $s^{-1}$. Each rill was manually incised along the plot maximum slope direction and then further shaped using a clear flow discharge of 0.1 L $s^{-1}$ which was applied for 3 min. Each rill was divided into 9 longitudinal segments defined by two cross-sections having a distance of 0.624 m. A rill reach is defined as the channel portion between a given measurement cross-section and the rill end. Measurements of bed slope, discharge, water depth, cross section area, wetted perimeter and flow velocity were carried out in 216 rill reaches.

A set of 70 photographs of the plot area and a 3D-photo reconstruction technique were used to obtain the 3D-DTM, applying the image-processing software Agisoft Photoscan Professional (version 1.1.6, Agisoft, Russia) (Frankl et al., 2015; Javernick et al., 2014; Seiz et al., 2006). The rill thalweg, extracted by 3D-DTM, was used to calculate the slope of each rill segment.

The water depth in a cross-section was measured by a micro-hydrometer located in the rill thalweg, constructed by a small aluminium rod (Figure 1), having a measurement accuracy of ±1 mm. The measured water depth and the geometric cross-section, obtained by 3D-DTM, allowed to calculate the cross-section area and wetted perimeter.

Flow velocity was measured by the dye tracing technique (Abrahams et al., 1996; Di Stefano et al., 2018b; Di Stefano et al., 2020a; Govers, 1992a; Line & Meyer, 1988) using a Methylene

**FIGURE 1** View of an experimental plot and micro-hydrometer used in this investigation

blue solution. A correction factor equal to 0.8 was used in the present experiments to convert the surface velocity $V_s$ to the mean flow velocity $V$ (Di Stefano et al., 2018b, 2020a; Li & Abrahamas, 1997; Luk & Merz, 1992; Zhang et al., 2010). However, few studies have been carried out to estimate mean flow velocity in rills (e.g., Abrahams et al., 1996; Di Stefano, Ferro, Palmeri, & Pampalone, 2017c; Rodrigo-Comino et al., 2017). To the best of our knowledge, the available studies on rill flow resistance (i.e., Govers, 1992a; Li et al., 1996) generally assumed a value of the correction factor without testing the effect of the uncertainty of this assumption on the Darcy-Weisbach friction factor. Recently, Di Stefano et al. (2018b) pointed out that the hypothesis on the correction factor value (0.665 or 0.8) has a quasi-negligible effect on the Darcy-Weisbach friction factor estimated for rill flows by Equation (19).

The experimental runs were carried out for Reynolds and Froude numbers corresponding to transitional and turbulent flow ($858 \le Re \le 14\,945$) and to subcritical and supercritical flow conditions ($0.47 \le F \le 1.95$) (Figure 2).

Further details are reported in the papers by Di Stefano et al. (2018a); Di Stefano, Nicosia, Palmeri, et al. (2019) and Palmeri et al. (2018).

## 3.2 | Experiments by Jiang et al. (2018)

The experiments by Jiang et al. (2018) were carried out in a rill flume, 0.12 m wide and 4 m long. The flume simulated a rill having a rectangular cross-section, with a non-erodible rough bed and fixed smooth sides, in which the sediment load of the flow was equal to its transport capacity.

The experiments were carried out by a colluvial soil, using seven slope gradients (Table 1) and five discharges in the range 0.0672–0.528 L $s^{-1}$. The investigated hydraulic conditions were characterized by transitional and turbulent flows ($639 \le Re \le 5529$) and supercritical flows ($1.57 \le F \le 8.14$) (Figure 2). Further details on the experimental apparatus and the measurement techniques are reported in the original paper.

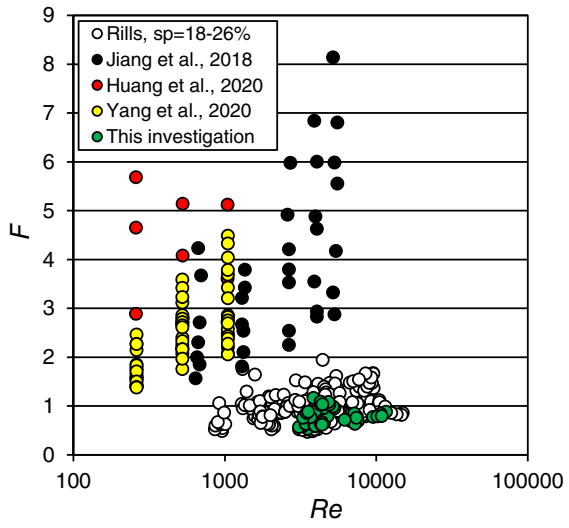


**FIGURE 2** Relationship between the Reynolds number *Re* and the Froude number *F* for the data base used in this investigation

## 3.3 | Experiments by Huang et al. (2020)

The experiments by Huang et al. (2020) were carried out in a rill flume comprising two slope sections: a sediment feeding section, 2.0-m long, 0.1-m wide and 0.15-m deep, located at the uppermost part of the soil flume and a sediment supply/settlement section 6.0 m long, 0.1 m wide and 0.35 m deep. Huang et al. (2020) conducted experiments in which eroded rills were fully developed and sediment load of the flow was equal to its transport capacity. The experimental runs were performed by a silt loam soil (23.8% sand, 64.6% silt and 11.6% clay), using three slope gradients (Table 1) and three discharges in the range 0.033–0.133 L $s^{-1}$. The investigated hydraulic conditions were characterized by flow Reynolds numbers ranging from 259 to 1043 and supercritical flows ($2.72 < F < 5.69$) (Figure 2). More details on the experimental apparatus and measurement techniques are reported in Huang et al. (2018, 2020).

## 3.4 | Experiments by Yang et al. (2020)

In this investigation the rill flume had a rectangular cross-section, 0.1 m wide and 0.4 m high, with an erodible rough bed and fixed smooth sides. The experimental runs were performed by a soil containing 4.35% sand, 69.78% silt and 25.87% clay particles and using four slope gradients (Table 1) and three discharges in the range 0.033–0.133 L $s^{-1}$. The hydrodynamic characteristics were affected by the changes in rill morphology due to the scour action of flow. The investigated hydraulic conditions were characterized by flow Reynolds numbers ranging from 261 to 1046 and supercritical flows ($1.38 < F < 4.49$) (Figure 2). Further details on the experimental flume and the measurement technique are reported in the paper by Yang et al. (2020).

## 3.5 | Experiments carried out in this investigation

In this investigation the measurement of discharge, water depth, cross-section area, wetted perimeter, bed slope and mean flow velocity were carried out for 47 reaches of experimental rills using the same equipment as Di Stefano et al. (2018a). The experimental runs were carried out using a clay loam soil (32.7% clay, 30.9% silt and 36.4% sand) (Table 1), a plot slope $s_p$ equal to 18% and values of reach slope $s$, due to the shaping flow action, greater than 0.16. The experimental runs were carried out using the same methods applied by Di Stefano et al. (2018a); Di Stefano, Nicosia, Palmeri, et al. (2019) and Palmeri et al. (2018).

For each experimental run, Table 2 lists the discharge $Q$, water depth $h$, the slope gradient $s$, the mean flow velocity $V$ and measured Darcy-Weisbach friction factor $f_m = 8\ g\ R\ s\ V^{-2}$.

**TABLE 2** Characteristic data of the experimental runs of the present investigation ($s_p = 18\%$)

| $Q$ / L s$^{-1}$ | $h$ / m | $s$ | $V$ / m s$^{-1}$ | $f_m$ |
|---|---|---|---|---|
| 0.24 | 0.016 | 0.179 | 0.276 | 1.675 |
| | 0.017 | 0.173 | 0.276 | 1.661 |
| | 0.016 | 0.173 | 0.274 | 1.646 |
| | 0.016 | 0.166 | 0.292 | 1.386 |
| 0.35 | 0.018 | 0.174 | 0.306 | 1.360 |
| | 0.018 | 0.178 | 0.316 | 1.288 |
| | 0.018 | 0.166 | 0.334 | 1.088 |
| 0.63 | 0.025 | 0.171 | 0.385 | 1.107 |
| | 0.024 | 0.161 | 0.383 | 1.030 |
| | 0.025 | 0.161 | 0.376 | 1.072 |
| 0.2 | 0.019 | 0.171 | 0.233 | 2.500 |
| | 0.017 | 0.169 | 0.240 | 1.991 |
| | 0.017 | 0.174 | 0.233 | 2.148 |
| | 0.017 | 0.174 | 0.256 | 1.727 |
| | 0.017 | 0.162 | 0.259 | 1.541 |
| 0.31 | 0.015 | 0.172 | 0.373 | 0.713 |
| | 0.015 | 0.175 | 0.342 | 0.847 |
| | 0.014 | 0.170 | 0.384 | 0.611 |
| | 0.012 | 0.163 | 0.403 | 0.459 |
| 0.41 | 0.017 | 0.175 | 0.392 | 0.796 |
| | 0.017 | 0.172 | 0.398 | 0.700 |
| | 0.016 | 0.171 | 0.402 | 0.659 |
| | 0.015 | 0.169 | 0.413 | 0.609 |
| | 0.014 | 0.168 | 0.399 | 0.629 |
| | 0.014 | 0.164 | 0.389 | 0.665 |
| 0.51 | 0.031 | 0.169 | 0.484 | 0.785 |
| | 0.030 | 0.172 | 0.456 | 0.888 |
| | 0.029 | 0.171 | 0.416 | 1.045 |
| | 0.030 | 0.168 | 0.430 | 0.983 |
| | 0.031 | 0.183 | 0.442 | 1.070 |
| 0.26 | 0.019 | 0.165 | 0.262 | 1.871 |
| | 0.020 | 0.164 | 0.257 | 1.982 |
| | 0.019 | 0.169 | 0.259 | 2.027 |
| | 0.019 | 0.160 | 0.290 | 1.456 |
| | 0.020 | 0.162 | 0.276 | 1.685 |
| | 0.020 | 0.162 | 0.277 | 1.707 |
| 0.34 | 0.016 | 0.177 | 0.302 | 1.267 |
| | 0.015 | 0.172 | 0.288 | 1.279 |
| | 0.014 | 0.167 | 0.318 | 0.989 |
| | 0.014 | 0.161 | 0.326 | 0.902 |
| 0.48 | 0.025 | 0.166 | 0.361 | 1.280 |
| | 0.024 | 0.165 | 0.352 | 1.304 |
| | 0.023 | 0.161 | 0.401 | 0.991 |
| 0.58 | 0.027 | 0.163 | 0.354 | 1.392 |
| | 0.028 | 0.171 | 0.332 | 1.688 |
| | 0.025 | 0.163 | 0.376 | 1.189 |
| | 0.023 | 0.163 | 0.341 | 1.392 |

*Note:* $s_p$, plot or flume slope.

The experimental values of the Reynolds and Froude number correspond to turbulent (3084 ≤ *Re* ≤ 11 586), subcritical and supercritical (0.53 ≤ *F* ≤ 1.17) flows.

### 3.6 | Characteristics of the data bases used for calibrating and testing the flow resistance law

All experimental runs used in this investigation (mobile bed rills and flumes with sediment transport) were carried out in small channels with flows having sediment transport. The data base is composed of flow resistance data on mobile bed rills incised in soil with a clay texture (216 experimental runs) (Di Stefano et al., 2018a; Di Stefano, Nicosia, Palmeri, et al., 2019; Palmeri et al., 2018), on rill flumes with a flow having a sediment load equal to its transport capacity (44 runs) (Huang et al., 2020; Jiang et al., 2018), on a rill flume with an erodible rough bed and fixed smooth sides (59 runs) (Yang et al., 2020) and on mobile bed rills (47 experimental runs) incised in a soil with a clay loam texture. Figures 2 and 3 show that the 366 measurements by Di Stefano et al. (2018a); Di Stefano, Nicosia, Palmeri, et al. (2019), Palmeri et al. (2018), Jiang et al. (2018), Huang et al. (2020), Yang et al. (2020) and those carried out in this investigation, cover a wide range of Reynolds (259 ≤ *Re* ≤ 14 945), Froude number (0.47 ≤ *F* ≤ 8.14) and plot/flume slope $s_p$ (17.6%–84%, Table 1). The data base constituted by the measurements of Di Stefano et al. (2018a); Di Stefano, Nicosia, Palmeri, et al. (2019), Palmeri et al. (2018), Jiang et al. (2018), Huang et al. (2020) was used to calibrate Equation (23). The 59 runs corresponding to the measurements by Yang et al. (2020), which are characterized by intermediate values of *Re*, *F* and *s* (Figure 3), and the 47 runs of the investigated clay loam soil were used as testing data base. The whole database is also characterized by different texture characteristics (Figure 4).

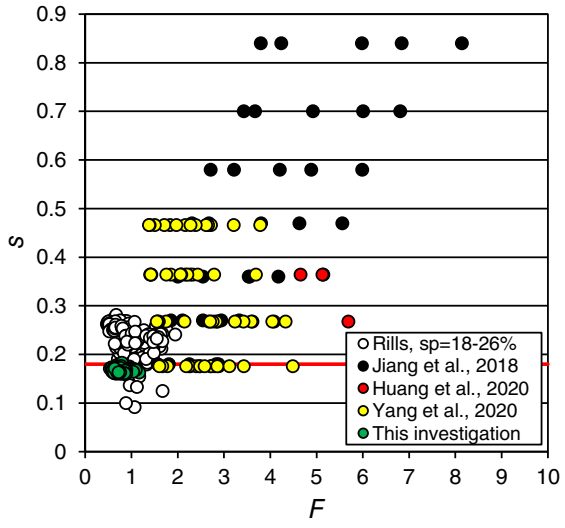


**FIGURE 3** Relationship between the Froude number *F* and the slope gradient *s* for the data base used in this investigation

## 4 | RESULTS

In accordance with previous results (Carollo et al., 2021; Palmeri et al., 2018), Equation (23) for estimating the $\Gamma_v$ function was first calibrated using the available data base (Table 1):

$$\Gamma_v = \left(0.4633\,\mathrm{CLAY}^{0.0652}\mathrm{SILT}^{0.0079}\right)\frac{F^{1.121}}{Re^{0.038}s^{0.6062}}. \quad (24)$$

Equation (24) is characterized by a coefficient of determination equal to 0.991, a mean square error MSE of 0.016 and is applicable for plot or flume slope in the range 18%–84%, 3 ≤ CLAY ≤ 71% and SILT ranging from 19.9% to 64.6%.

The comparison between the 260 measured $\Gamma_v$ values of the calibrating data set, obtained by Equations (20) and (21), and those calculated applying Equation (24) is plotted in Figure 5.

Coupling Equations (24) and (9) the following flow resistance law was obtained:

$$f = 8\left[\frac{(\delta+1)(\delta+2)}{2^{1-\delta}Re^{\delta}}\left(\frac{1}{0.4633\,\mathrm{CLAY}^{0.0652}\mathrm{SILT}^{0.0079}}\right)\frac{Re^{0.038}s^{0.6062}}{F^{1.121}}\right]^{\frac{2}{1+\delta}}. \quad (25)$$

Equation (25) demonstrates that the friction factor *f* depends on the percentage of clay and silt of the soil in which the rills are shaped. From a physical point of view, being the silt fraction constituted by particles which can be easily detached from the soil mass, it can be assumed as representative of the soil detachability effect on flow resistance. Moreover, the primary clay particles, corresponding to CLAY, are easily transportable and consequently the clay fraction expresses the effect of soil particle transportability on flow resistance. Equation (25) also demonstrates that Reynolds number takes into account that (i) the velocity distribution is affected by flow regime and (ii) the considered wide experimental range (259–14 945) makes it useful to be applied for different flow regimes.

The good agreement between the measured Darcy-Weisbach friction factor values of the calibrating data base and those calculated by the theoretical flow resistance equation (Equation 25) is shown in Figure 6. The friction factor values calculated by Equation (25) are characterized by errors $E = 100\,(f - f_m)/f_m$ that are less than or equal to ±20% for 98.1% of cases and less than or equal to ±10% for 78.1% of cases.

Figure 7 shows that the 260 *E* values are distributed according to a normal law with mean value and standard deviation equal to 0.36 and 8.7, respectively. The statistical hypothesis that *E* is normally distributed was positively tested by the Kolgomorov-Smirnov test for a probability level equal to 0.05. In other words, Equation (25) is a 'complete' flow resistance model for estimating the Darcy-Weisbach friction factor and no variable affecting the physical process was neglected.

Figure 8 shows the comparison between the measured $\Gamma_v$ values obtained by Equations (20) and (21), and those calculated applying Equation (24) for the independent testing data set (i.e., data by Yang et al. (2020) and this investigation, Table 2).

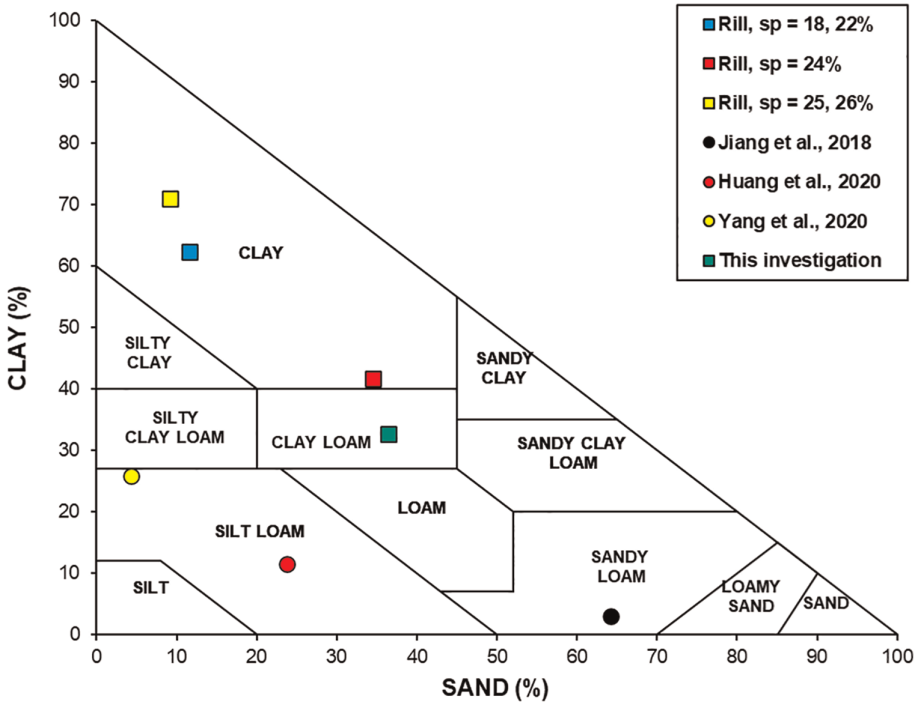


**FIGURE 4** Texture classification of the investigated soils

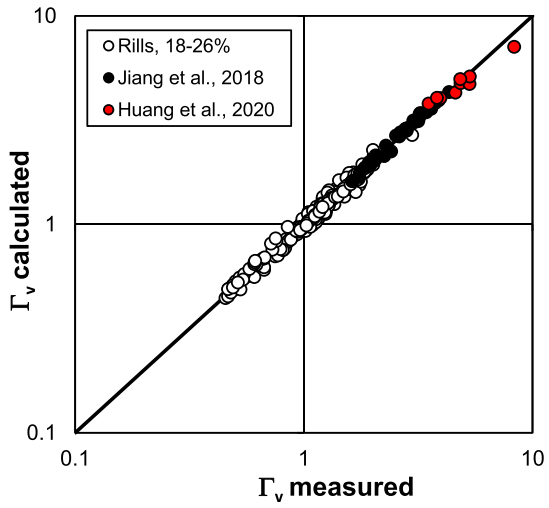


**FIGURE 5** Comparison between the measured $\Gamma_v$ values obtained by Equations (20) and (21) and those calculated by Equation (24) for calibration data base

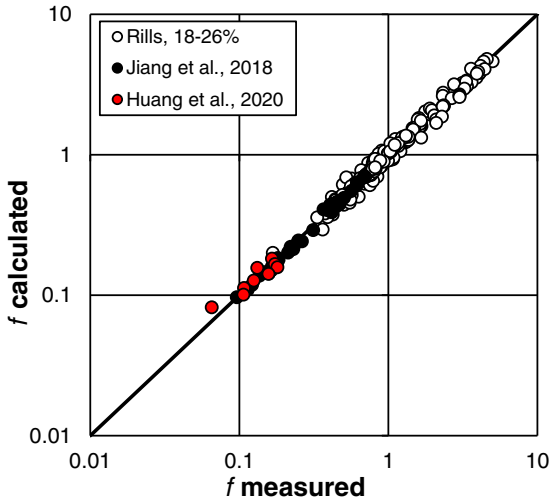


**FIGURE 6** Comparison between measured Darcy-Weisbach friction factor values and those calculated by Equation (25) for calibration data base

The good agreement between the measured Darcy-Weisbach friction factor $f_m$ values and those $f$ calculated by the theoretical flow resistance equation (Equation 25) for the testing dataset is shown in Figure 9. The latter are characterized by errors $E$ less than or equal to ±20% for 87.7% of cases and less than or equal to ±10% for 32.1% of cases.

Into Equation (25) the effect of the soil transportability and detachability can be expressed by the following index of sediment transport STI:

$$\mathrm{STI} = \frac{1}{0.4633\,\mathrm{CLAY}^{0.0652}\mathrm{SILT}^{0.0079}}. \quad (26)$$

Figure 10, which shows the relationship between STI and CLAY as an example for three sand contents of 20%, 33% and 40%, highlights that the sand content does not appreciably affects the sediment transport index values within the investigated clay range.

Figure 11 shows the relationship between the Reynolds number and the ratio $2c\,(\delta+1)^{-1}$, with $c = 0.6062$, which is the exponent of the slope gradient in Equation (25). This figure demonstrates that, for the available data base of this investigation (366 experimental runs), the exponent of the slope gradient assumes values ranging from 0.95 to 1.05 with a mean of 1.01.

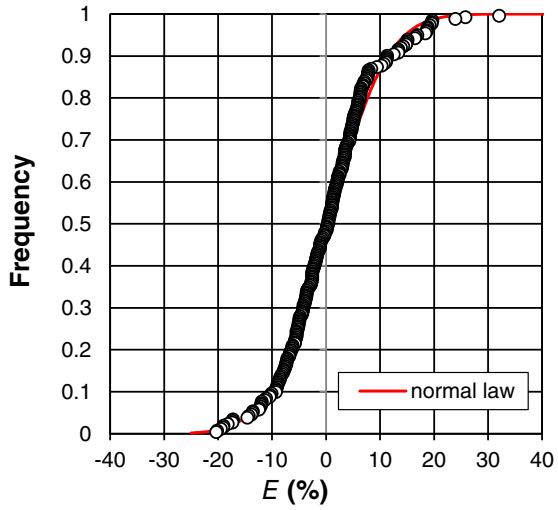


FIGURE 7 Frequency distribution of the errors $E$

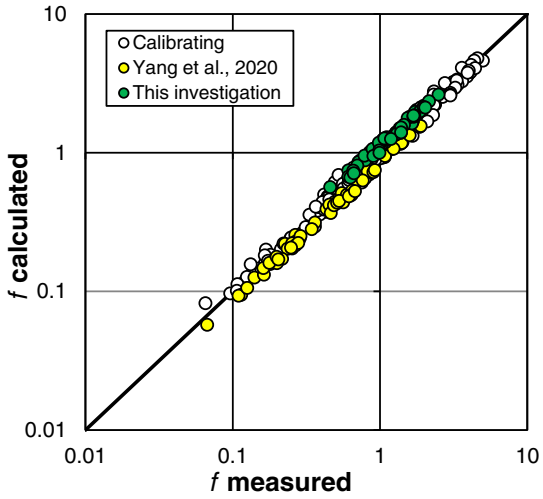


FIGURE 9 Comparison between measured Darcy-Weisbach friction factor values and those calculated by Equation (25) for testing data base

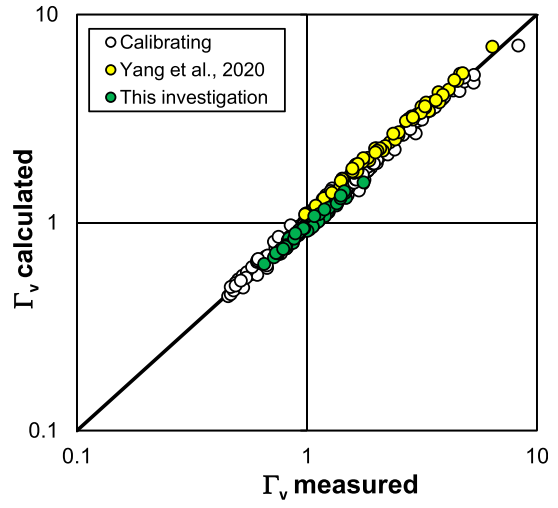


FIGURE 8 Comparison between the measured $\Gamma_v$ values obtained by Equations (20) and (21) and those calculated by Equation (24) for testing data base

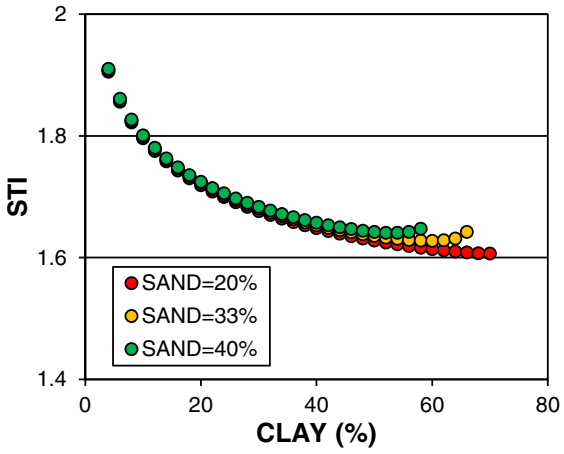


FIGURE 10 Relationship, as an example for a sand fraction of 20%, 33% and 40%, between the sediment transport index STI and the clay content

Taking into account that $Re^{\delta}$ is equal to 4.4817 and using the mean value of $\delta$ (0.187) as its experimental range (0.156–0.27) is narrow, Equation (25) can be rewritten as:

$$f = 4.505 \frac{1}{\mathrm{CLAY}^{0.110}\mathrm{SILT}^{0.013}} \frac{Re^{0.064}\, s^{1.022}}{F^{1.889}}. \quad (27)$$

The obtained results highlight the following key-findings: (1) the soil texture, represented by clay and silt fraction, affects the estimate of the $\Gamma$ parameter and the theoretical flow resistance law, (2) the proposed Equation (24) is positively tested using independent rill measurements carried out for a plot slope equal to 18% and literature data, (3) the estimate of the Darcy-Weisbach friction factor (Equation 25) is affected by the soil particle detachability and transportability and (4) the Darcy-Weisbach friction factor is linearly related to the rill slope.

## 5 | DISCUSSION

Equation (24), which relates $\Gamma_v$ with hydraulic conditions represented by $Re$ and $F$, slope and soil textural data, is characterized by a wide range of applicability in terms of flow regime (Figure 2), flow characteristics ($0.47 \le F \le 8.14$) and plot or flume slope ($18 \le s_p \le 84\%$). The analysis demonstrated that texture information of the investigated soils, like clay and silt fractions, are required for taking into account the effect of detachment and transport of soil particles on rill flow velocity.

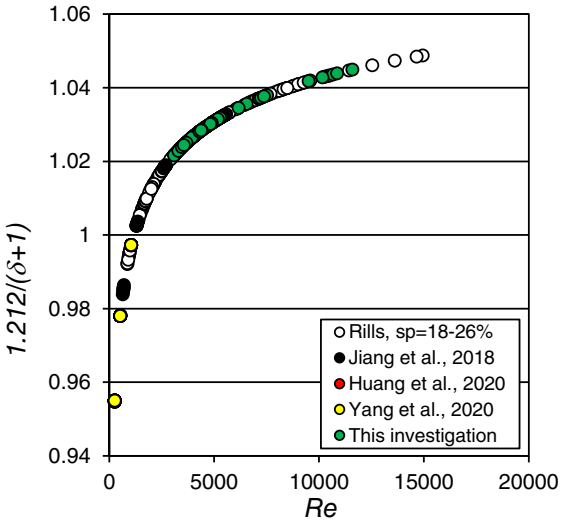


**FIGURE 11** Relationship between the Reynolds number and the exponent of the slope gradient in Equation (25)

At present, limited information on the effect of sediment transport on rill flow resistance is available. Di Stefano, Nicosia, Pampalone, et al. (2019) using the measurements by Jiang et al. (2018) established that flow resistance increases with bed load transport, in accordance with the available results for open channel flows (Gao & Abrahams, 2004). Furthermore, the impact of the overall (i.e., bed load and suspended) sediment transport on the rill flow resistance should be significantly lower than that of the grain roughness (Di Stefano, Nicosia, Palmeri, et al., 2019).

The actual sediment transport is the result of the interaction between the flow characteristics, which are represented by the sediment transport capacity $T_c$ (Ferro, 1998), and soil particle properties. These are described by the attitude of soil particles to be detached from the rill wetted perimeter (detachability) and transported (transportability). The properties of the eroded particles including grain size, particle shape, specific weight, organic matter content, mineralogy and aggregate stability influence the sediment delivery processes. Soil particles detached by water erosion processes result in a mixture of primary particles and aggregates and are transported as compound particles (Liu et al., 2019). Results presented by Meyer, Foster, and Nikolov (1975); Meyer, Foster, and Römkens (1975) indicated that about 15% of the particles transported in rill flow from a tilled soil were larger than 1 mm and almost 3% of the sediment eroded was larger than 5 mm, indicating that rill flow should be able to transport large particles (Di Stefano & Ferro, 2002).

Several research efforts have been made to detect the influence of different hydraulic parameters, such as unit discharge, mean flow velocity and slope on $T_c$ (Abrahams et al., 2001; Ali et al., 2011, 2012; Beasley & Huggins, 1982; Everaert, 1991; Ferro, 1998; Finkner et al., 1989; Govers, 1990, 1992b; Govers & Rauws, 1986; Guy et al., 1990; Julien & Simons, 1985; Prosser & Rustomji, 2000; Wu et al., 2016; Xiao et al., 2017; Zhang et al., 2009). The results obtained by Ali et al. (2011, 2012) for erodible beds clearly showed that slope gradient has a strong impact on sediment transport capacity and this circumstance was attributed to the increase of the tangential component of the gravity force with slope gradient. Many studies demonstrated that sediment transport capacity increases as a power function of slope gradient (Xiao et al., 2017) and its exponent varied within a range of 0.9–1.8 (Prosser & Rustomji, 2000; Zhang et al., 2011). Previous research demonstrated that the relationship between transport capacity and unit discharge is always dependent on slope (Ali et al., 2011; Prosser & Rustomji, 2000; Zhang et al., 2009) and that the effect of unit discharge and slope on $T_c$ is affected by erodible to non-erodible bed conditions (Zhang et al., 2009). In particular, for given hydraulic and sediment conditions, the roughness of non-erodible beds is always less than that of erodible beds and for this last condition the effect of slope on transport capacity is higher than the effect of unit discharge (Everaert, 1991; Govers, 1990).

According to these observations, for steep slopes (i.e., for slope gradients greater than or equal to 18%) the high sediment transport capacity is not a limiting factor for the actual sediment transport. Consequently, the actual sediment transport in rills on steep slopes can be limited only by the detachability of soil particles from the soil mass or the transportability of the eroded particles.

Equation (25) shows that the exponent of SILT fraction is almost equal to zero demonstrating that the effect of the soil particle detachability is negligible respect to that of the transportability.

Also, Equation (25) with STI values shown in Figure 10 allows to deduce that, for given slope, hydraulic conditions and sand fraction, $f$ decreases as CLAY increases. Therefore, $f$ is inversely related to transportability of soil particles in steep slopes. For the steep slope condition, in which $T_c$ is not a limiting factor of the actual sediment transport, the soil characteristics and in particular the soil transportability, exert the main influence on the energy dissipation due to sediment transport. When the clay fraction increases detached particles are easily transported, and this condition implies that a low rate of flow energy is used for sediment transport. Furthermore, clay particles are transported as suspended sediments and experimental results (Vanoni & Nomicos, 1959) indicate that the suspended load reduces the friction factor by damping flow turbulence. Vanoni and Nomicos (1959) suggested that when a sediment laden flow moves fast on a flat bed the friction factor is lower than that of a clear flow moving on a fixed bed of comparable roughness. Vanoni (1946) suggested that the Darcy –Weisbach friction factor decreases in presence of suspended sediment load and this hypothesis was recently confirmed by Di Stefano et al. (2020b) which tested the theoretical flow resistance Equation (19) using literature measurements carried out by flume investigations with suspended sediment-laden flows.

In agreement with previous studies (Di Stefano et al., 2018a; Di Stefano, Ferro, Palmeri, & Pampalone, 2017c; Di Stefano, Nicosia, Palmeri, et al., 2019; Palmeri et al., 2018), Figure 11 and Equation (27) demonstrate that the Darcy-Weisbach friction factor $f$ increases with a power of slope gradient having an exponent close to 1. This result confirms, for the steep slope case, the hypothesis of Govers (1992a)

that flow velocity is quasi-independent of slope in mobile bed rills. This result is physically explained for mobile-bed rills on steep slopes by the well-known 'feedback mechanism' which assures that when slope gradient increases the expected increase of flow velocity is counterbalanced by the increase of bed roughness due to a more active rill erosion process.

Notwithstanding the flow resistance Equation (25) is characterized by a wide range of applicability in terms of flow regime, Froude number and slope, the main limitations of the proposed approach are related to (i) the adopted power shape of the velocity profile, (ii) the ability of clay and silt fractions to represent the effect of detachment and transport of soil particles on rill flow velocity, (iii) neglect the influence of soil aggregation on transported sediment as flow actually contains a mixture of primary particles and aggregates.

## 6 | CONCLUSIONS

Previous research suggests that for mobile bed rills the classical hydraulic formulations, as equations by Chezy or Manning, do not consider the effects of interaction between flow, bed morphology and sediment transport.

Previous data on mobile bed rill channels joined with measurements carried out in rill flumes, in which the sediment load of the flow was equal to its transport capacity, were used for testing the applicability of a theoretical rill flow resistance law. This database was constituted by measurements characterized by high slope values ($s_p$ ranging from 17.6% to 84%) and a wide range of textural fractions.

Considering that the actual sediment transport in rills on steep slopes is not limited by sediment transport capacity and can be limited only by the detachability of soil particles from the soil mass or the transportability of the eroded particles, the developed analysis established that Darcy-Weisbach friction factor is affected by silt and clay fraction of the investigated soil. The measurements confirmed that the Darcy-Weisbach friction factor can be accurately estimated by the proposed theoretical approach.

The developed analysis for the steep slope condition pointed out that the soil characteristics, and in particular the soil transportability represented by clay fraction, exert the main influence on the energy dissipation. Furthermore, considering that clay particles are transported as suspended sediments, the obtained results, in agreement with previous studies, indicated that the suspended load reduces the friction factor.

Finally, the analysis on the exponent of the slope gradient in the flow resistance equation confirmed the hypothesis of Govers (1992a) that flow velocity in mobile bed rills is quasi-independent of slope.

### ACKNOWLEDGEMENTS

All authors contributed to outline the investigation, analyse the data, discuss the results and write the manuscript.

### DATA AVAILABILITY STATEMENT

The data that support the findings of this study are available in this paper (Table 2) or previously published papers.

### ORCID

*Alessio Nicosia* https://orcid.org/0000-0003-0540-8788
*Vincenzo Palmeri* https://orcid.org/0000-0001-6594-9530
*Vincenzo Pampalone* https://orcid.org/0000-0002-5195-9209
*Vito Ferro* https://orcid.org/0000-0003-3020-3119

### REFERENCES

Abrahams, A. D., Li, G., Krishana, C., & Atkinson, J. F. (2001). A sediment transport equation for interrill overland flow on rough surface. *Earth Surface Processes and Landforms*, *26*, 1443–1459.

Abrahams, A. D., Li, G., & Parsons, A. J. (1996). Rill hydraulics on a semiarid hillslope, southern Arizona. *Earth Surface Processes and Landforms*, *21*, 35–47.

Ali, M., Seeger, M., Sterk, G., Seeger, M., Boersema, M. P., & Peters, P. (2013). A unit stream power based sediment transport function for overland flow. *Catena*, *101*, 197–204.

Ali, M., Sterk, G., Seeger, M., Boersema, M., & Peters, P. (2012). Effect of hydraulic parameters on sediment transport capacity in overland flow over erodible beds. *Hydrology and Earth System Sciences*, *16*, 591–601. https://doi.org/10.5194/hess-16-591-2012

Ali, M., Sterk, G., Seeger, M., & Stroosnijder, L. (2011). Effect of hydraulic parameters on sediment transport capacity in overland flow over erodible beds. *Hydrology and Earth System Sciences*, *8*(4), 6939–6965.

Bagarello, V., Di Stefano, C., Ferro, V., & Pampalone, V. (2015). Establishing a soil loss threshold for limiting rilling. *Journal of Hydrologic Engineering, ASCE*, *20*(C6014001), 1–5.

Bagarello, V., & Ferro, V. (2004). Plot-scale measurements of soil erosion at the experimental area of Sparacia (southern Italy). *Hydrological Processes*, *18*, 141–157.

Bagarello, V., & Ferro, V. (2010). Analysis of soil loss data from plots of different length for the Sparacia experimental area, Sicily, Italy. *Byosystems Engineering*, *105*, 411–422.

Baiamonte, G., Ferro, V., & Giordano, G. (1995). Advances on velocity profile and flow resistance law in gravel bed rivers. *Excerpta*, *9*, 41–89.

Barenblatt, G. I. (1979). *Similarity, self-similarity and intermediate asymptotics*. Consultants Bureau.

Barenblatt, G. I. (1987). *Dimensional analysis*. Gordon & Breach, Science Publishers Inc.

Barenblatt, G. I. (1991). On the scaling laws (incomplete self-similarity with respect to Reynolds numbers) for the developed turbulent flows in tubes. *Compets Rendus de Academie des Sciences Series II*, *313*, 307–312.

Barenblatt, G. I. (1993). Scaling laws for fully developed turbulent shear flows, part 1, basic hypothesis and analysis. *Journal of Fluid Mechanics*, *248*, 513–520.

Barenblatt, G. I., & Monin, A. S. (1979). Similarity laws for turbulent stratified flows. *Archive for Rational Mechanics and Analysis*, *70*, 307–317.

Barenblatt, G. I., & Prostokishin, V. M. (1993). Scaling laws for fully developed turbulent shear flows, part 2. Processing of experimental data. *Journal of Fluid Mechanics*, *248*, 521–529.

Beasley, D. B., & Huggins, L. F. (1982). *ANSWERS user's manual*. Department of Agricultural Engineering.

Bennett, S. J., Gordon, L. M., Neroni, V., & Wells, R. R. (2015). Emergence, persistence, and organization of rill network. *Natural Hazards*, *79*, S7–S24. https://doi.org/10.1007/s11069-015-1599-8

Borrelli, P., Robinson, D. A., Fleischer, L. R., Lugato, E., Ballabio, C., Alewell, C., Meusburger, K., Modugno, S., Schutt, B., Ferro, V., Bagarello, V., Van Oost, K., Montanarella, L., & Panagos, P. (2017). An assessment of the global impact of the 21st century land use change on soil erosion. *Nature Communications*, *8*, 1–13.

Bruno, C., Di Stefano, C., & Ferro, V. (2008). Field investigation on rilling in the experimental Sparacia area, South Italy. *Earth Surface Processes and Landforms*, *33*, 263–279.

Butera, L., Ridolfi, L., & Sordo, S. (1993). On the hypothesis of selfsimilarity for the velocity distribution in turbulent flows. *Excerpta*, *8*, 63–94.

Carollo, F. G., Di Stefano, C., Ferro, V., & Pampalone, V. (2015). Measuring rill erosion at plot scale by a drone-based technology. *Hydrological Processes*, *29*(17), 3802–3811.

Carollo, F. G., Di Stefano, C., Nicosia, A., Palmeri, V., Pampalone, V., & Ferro, V. (2021). Flow resistance in mobile bed rills shaped in soils with different texture. *European Journal of Soil Science*, 1–14. https://doi.org/10.1111/ejss.13093

Castaing, B., Gagne, Y., & Hopfinger, E. J. (1990). Velocity probability density functions of high Reynolds number turbulence. *Physica D*, *46*, 177–200.

Di Stefano, C., & Ferro, V. (2002). Linking clay enrichment and sediment delivery processes. *Biosystems Engineering*, *81*, 465–479.

Di Stefano, C., & Ferro, V. (2016). Establishing soil loss tolerance: An overview. *Journal of Agricultural Engineering Research*, *XLVII*, 127–133.

Di Stefano, C., Ferro, V., Palmeri, V., & Pampalone, V. (2017b). Measuring rill erosion using structure from motion: A plot experiment. *Catena*, *153*, 383–392.

Di Stefano, C., Ferro, V., Palmeri, V., & Pampalone, V. (2017c). Flow resistance equation for rills. *Hydrological Processes*, *31*, 2793–2801.

Di Stefano, C., Ferro, V., Palmeri, V., & Pampalone, V. (2018a). Testing slope effect on flow resistance equation for mobile bed rills. *Hydrological Processes*, *32*, 664–671.

Di Stefano, C., Ferro, V., Palmeri, V., & Pampalone, V. (2018b). Assessing dye-tracer technique for rill flow velocity measurements. *Catena*, *171*, 523–532.

Di Stefano, C., Ferro, V., Palmeri, V., Pampalone, V., & Agnello, F. (2017). Testing the use of an image-based technique to measure gully erosion at Sparacia experimental area. *Hydrological Processes*, *31*, 573–585.

Di Stefano, C., Ferro, V., & Pampalone, V. (2015). Modeling rill erosion at the Sparacia experimental area. *Journal of Hydrologic Engineering*, *ASCE*, *20*(C5014001), 1–12.

Di Stefano, C., Ferro, V., Pampalone, V., & Sanzone, F. (2013). Field investigation of rill and ephemeral gully erosion in the Sparacia experimental area, South Italy. *Catena*, *101*, 226–234.

Di Stefano, C., Nicosia, A., Palmeri, V., Pampalone, V., & Ferro, V. (2019). Comparing flow resistance law for fixed and mobile bed rills. *Hydrological Processes*, *33*, 3330–3348.

Di Stefano, C., Nicosia, A., Palmeri, V., Pampalone, V., & Ferro, V. (2020a). Dye-tracer technique for rill flows by velocity profile measurements. *Catena*, *185*, 104313.

Di Stefano, C., Nicosia, A., Palmeri, V., Pampalone, V., & Ferro, V. (2020b). Flow resistance law under suspended sediment laden conditions. *Flow Measurement and Instrumentation*, *74*, 101771.

Di Stefano, C., Nicosia, A., Pampalone, V., Palmeri, V., & Ferro, V. (2019). Rill flow resistance law under equilibrium bed-load transport conditions. *Hydrological Processes*, *33*, 1317–1323.

Everaert, W. (1991). Empirical relations for the sediment transport capacity of interrill flow. *Earth Surface Processes and Landforms*, *16*, 513–532.

Ferro, V. (1997). Applying hypothesis of self-similarity for flow-resistance law of small-diameter plastic pipes. *Journal of Irrigation and Drainage Engineering*, *ASCE*, *123*, 175–179.

Ferro, V. (1998). Evaluating overland flow sediment transport capacity. *Hydrological Processes*, *12*, 1895–1910.

Ferro, V. (1999). Friction factor for gravel-bed channel with high boulder concentration. *Journal of Hydraulic Engineering*, *ASCE*, *125*, 771–778.

Ferro, V. (2003). ADV measurements of velocity distribution in a gravel bed flume. *Earth Surface Processes and Landforms*, *28*, 707–722.

Ferro, V. (2017). New flow resistance law for steep mountain streams based on velocity profile. *Journal of Irrigation and Drainage Engineering*, *ASCE*, *143*(04017024), 1–6.

Ferro, V. (2018). Assessing flow resistance in gravel bed channels by dimensional analysis and self-similarity. *Catena*, *169*, 119–127.

Ferro, V., & Baiamonte, G. (1994). Flow velocity profiles in gravel bed rivers. *Journal of Hydraulic Engineering*, *ASCE*, *120*, 60–80.

Ferro, V., & Pecoraro, R. (2000). Incomplete self-similarity and flow velocity in gravel bed channels. *Water Resources Research*, *36*, 2761–2770.

Ferro, V., & Porto, P. (2018). Applying hypothesis of self-similarity for flow resistance law in Calabrian gravel bed rivers (Fiumare). *Journal of Hydraulic Engineering*, *ASCE*, *144*, 1–11.

Finkner, S. C., Nearing, M. A., Foster, G. R., & Gilley, J. E. (1989). A simplified equation for modeling sediment transport capacity. *Transactions of the ASAE*, *32*, 1545–1550.

Foster, G.R., Flanagan, D.C., Nearing, M.A., Lane, L.J., Risse, L.M., & Finkner, S. C. (1995). Hillslope erosion component. In D. C. Flanagan & M. A. Nearing (Eds.), USDA water erosion prediction project hillslope profile and watershed model documentation. NSERL report no. 10. USDA-ARS National Soil Erosion Research Laboratory, West Lafayette, Ind. 12 pp.

Foster, G. R., Huggins, L. F., & Meyer, L. D. (1984). A laboratory study of rill hydraulics: I. velocity relationships. *Transactions of the ASAE*, *27*, 790–796.

Frankl, A., Stal, C., Abraha, A., Nyssen, J., Rieke-Zapp, D., De Wulf, A., & Poesen, J. (2015). Detailed recording of gully morphology in 3D through image-based modelling. *Catena*, *127*, 92–101.

Gao, P., & Abrahams, A. D. (2004). Bedload transport resistance in rough open-channel flows. *Earth Surface Processes and Landforms*, *29*, 423–435.

Gilley, J. E., Kottwitz, E. R., & Simanton, J. R. (1990). Hydraulics characteristics of rills. *Transactions of the ASAE*, *27*, 797–804.

Giménez, R., & Govers, G. (2001). Interaction between bed roughness and flow hydraulics in eroding rills. *Water Resources Research*, *37*, 791–799.

Gómez-Gutiérrez, A., Schnabel, S., Berenguer-Sempere, F., Lavado-Contador, F., & Rubio-Delgado, J. (2014). Using 3D photo-reconstruction methods to estimate gully headcut erosion. *Catena*, *120*, 91–101.

Govers, G. (1990). Empirical relationships on the transporting capacity of overland flow. *Transport and Deposition Processes*, *Proceedings of the Jerusalem Workshop*, *March–April 1987*, *IAHS*, *189*, 45–63.

Govers, G. (1992a). Relationship between discharge, velocity and flow area for rills eroding loose, non -layered materials. *Earth Surface Processes and Landforms*, *17*, 515–528.

Govers, G. (1992b). Evaluation of transporting capacity formulae for overland flow. In A. J. Parsons & A. D. Abrahams (Eds.), Overland flow hydraulics and erosion mechanics, University College London Press, London, 243–273.

Govers, G., Giménez, R., & Van Oost, K. (2007). Rill erosion: Exploring the relationship between experiments, modeling and field observations. *Earth Science Reviews*, *8*, 87–102.

Govers, G., & Rauws, G. (1986). Transporting capacity of overland flow on plane and on irregular beds. *Earth Surface Processes and Landforms*, *11*, 515–524.

Guy, B. T., Dickinson, W. T., Rudra, R. P., & Wall, G. J. (1990). Hydraulics of sediment-laden sheetflow and the influence of simulated rainfall. *Earth Surface Processes and Landforms*, *15*, 101–118.

Hessel, R., Jetten, V., & Guanghui, Z. (2003). Estimating manning's n for steep slopes. *Catena*, *54*, 77–91.

Huang, Y., Li, F., Liu, Z., Li, J., & Gao, X. (2020). Experimental determination of sediment transport capacity of concentrated water flow over saturated soil slope. *European Journal of Soil Science*, *72*(2), 756–768. https://doi.org/10.1111/ejss.12989

Huang, Y. H., Chen, X. Y., Li, F. H., Zhang, J., Lei, T. W., Li, J., Chen, P., & Wang, X. F. (2018). Velocity of water flow along saturated loess slopes under erosion effects. *Journal of Hydrology*, *561*, 304–311.

James, M. R., & Robson, S. (2012). Straightforward reconstruction of 3D surfaces and topography with a camera: Accuracy and geosciences applications. *Journal of Geophyisical Research*, *117*, 1–17.

Javernick, L., Brasington, J., & Caruso, B. (2014). Modeling the topography of shallow braided rivers using structure-from-motion photogrammetry. *Geomorphology*, *213*, 166–182.

Jiang, F., Gao, P., Si, X., Zhan, Z., Zhang, H., Lin, J., Ji, X., Wang, M. K., & Huang, Y. (2018). Modelling the sediment transport capacity of flows in nonerodible rills. *Hydrological Processes*, *32*, 3852–3865.

Julien, P. Y., & Simons, D. B. (1985). Sediment transport capacity of overland flow. *Transactions of the ASAE*, *28*, 755–762.

Li, G., & Abrahamas, A. D. (1997). Effect of salting sediment load on the determination of the mean velocity of overland flow. *Water Resources Research*, *33*, 341–347.

Li, G., Abrahams, A. D., & Atkinson, J. F. (1996). Correction factors in the determination of mean flow velocity of overland flow. *Earth Surface Processes and Landforms*, *21*, 509–515.

Line, D. E., & Meyer, L. D. (1988). Flow velocities of concentrated runoff along cropland furrows. *Transactions of the ASAE*, *31*, 1435–1439.

Liu, G., Dabney, S., Yoder, D., Wells, R., & Vieira, D. (2019). Modeling land management effects on the size distribution of eroded sediment. *Soil & Tillage Research*, *192*, 121–133.

Luk, S. H., & Merz, W. (1992). Use of the salt tracing technique to determine the velocity of overland flow. *Soil Technology*, *5*, 289–301.

Meyer, L. D., Foster, G. R., & Nikolov, S. (1975). Effect of flow rate and canopy on rill erosion. *Transactions of the ASAE*, *18*, 905–911.

Meyer, L.D., Foster, G.R., & Römkens, M.J.M. (1975). Source of soil eroded by water from upland slopes. In Present and prospective technology of predicting sediment yields and sources, agriculture research service report, ARS-S-40,177-189.

Micheletti, N., Chandler, J. H., & Lane, S. N. (2015). Structure from motion (SfM) photogrammetry. *Photogrammetric Heritage*, *2*, 1–12.

Mutchler, C.K., & Young, R.A. (1975). Soil detachment by raindrops. In Present and prospective technology for predicting sediment yields and sources ARS-S-40, pp. 113–117.

Nearing, M. A., Norton, L. D., Bulgakov, D. A., Larionov, G. A., West, L. T., & Dontsova, K. M. (1997). Hydraulics and erosion in eroding rills. *Water Resources Research*, *33*, 865–876.

Nearing, M. A., Simanton, J. R., Norton, L. D., Bulygin, S. J., & Stone, J. (1999). Soil erosion by surface water flow on a stony, semiarid hillslope. *Earth Surface Processes and Landforms*, *24*, 677–686.

Nicosia, A., Di Stefano, C., Palmeri, V., Pampalone, V., Ferro, V., & Nearing, M. A. (2019). Testing a new rill flow resistance approach using the water erosion prediction project experimental database. *Hydrological Processes*, *33*, 616–626.

Nouwakpo, S. K., Williams, C. J., Al-Hamdam, O. Z., Weltz, M. A., Pierson, F., & Nearing, M. (2016). A review of concentrated flow erosion processes on rangelands: Fundamental understanding and knowledge gaps. *International Soil and Water Conservation Research*, *4*, 75–86.

Palmeri, V., Pampalone, V., Di Stefano, C., Nicosia, A., & Ferro, V. (2018). Experiments for testing soil texture effects on flow resistance in mobile bed rills. *Catena*, *171*, 176–184.

Peng, W., Zhang, Z., & Zhang, K. (2015). Hydrodynamic characteristics of rill flow on steep slopes. *Hydrological Processes*, *29*, 3677–3686.

Powell, D. M. (2014). Flow resistance in gravel-bed rivers: Progress in research. *Earth-Science Reviews*, *136*, 301–338.

Prosser, I., & Rustomji, P. (2000). Sediment transport capacity relations for overland flow. *Progress in Physical Geography*, *24*, 179–193.

Rodrigo-Comino, J., Wirtz, S., & Brevik, E. C. (2017). Assessment of agri-spillways as a soil erosion protection measure in Mediterranean sloping vineyards. *Journal of Mountain Science*, *14*, 1009–1022.

Seiz, S.M., Curless, B., Diebel, J., Scharstein, D., & Szeliski, R. (2006). A comparison an evaluation of multi-view stereo reconstruction algorithms. Paper presented at IEEE conference on computer vision ad pattern recognition. IEEE Computer Society, New York, N.Y.

Strohmeier, S. M., Nouwakpo, S. K., Huang, C. H., & Klik, A. (2014). Flume experimental evaluation of the effect of rill flow path tortuosity on rill roughness based on the Manning-Strickler equation. *Catena*, *118*, 226–233.

Stroosnijder, L. (2005). Measurement of erosion: Is it possible? *Catena*, *64*, 162–173.

Takken, I., & Govers, G. (2000). Hydraulics of interrill overland flow on rough, bare soil surfaces. *Earth Surface Processes and Landforms*, *25*, 1387–1402.

Takken, I., Govers, G., Ciesiolka, C. A. A., Silburn, D. M., & Loch, R. J. (1998). Factors influencing the velocity-discharge relationship in rills. In *Modeling soil erosion, sediment transport and closely related hydrological processes* (Vol. 249, pp. 63–69). IAHS Publication.

Thomsen, L. M., Baartman, J. E. M., Barneveld, R. J., Starkloff, T., & Stolte, J. (2015). Soil surface roughness: Comparing old and new measuring methods and application in a soil erosion model. *The Soil*, *1*(1), 399–410.

Torri, D., Poesen, J., Borselli, L., Bryan, R., & Rossi, M. (2012). Spatial variation of bed roughness in eroding rills and gullies. *Catena*, *90*, 76–86.

Vanoni, V. A. (1946). Transportation of suspended sediment by water. *Transactions of the American Society of Civil Engineers, ASCE*, *111*, 67–133.

Vanoni, V. A., & Nomicos, G. N. (1959). Resistance properties of sediment-laden streams. *J. Hydraulics Division, ASCE*, *85*, 77–107.

Wang, P., Yao, J., Wang, G., Hao, F., Shrestha, S., Xue, B., Xie, G., & Peng, Y. (2019). Exploring the application of artificial intelligence technology for identification of water pollution characteristics and tracing the source of water quality pollutants. *Science of the Total Environment*, *693*, 133440.

Wang, Z., Yang, X., Liu, J., & Yuan, Y. (2015). Sediment transport capacity and its response to hydraulic parameters in experimental rill flow on steep slope. *Journal of Soil and Water Conservation*, *70*(1), 36–44.

Westoby, M. J., Brasington, J., Glasser, N. F., Hambrey, M. J., & Reynolds, J. M. (2012). 'Structure-from-motion' photogrammetry: A low-cost, effective tool for geoscience applications. *Geomorphology*, *179*, 300–314.

Wirtz, S., Seeger, M., Remke, A., Wengel, R., Wagner, J., & Ries, J. B. (2013). Do deterministic sediment detachment and transport equations adequately represent the process-interactions in eroding rills? An experimental field study. *Catena*, *101*, 61–78.

Wirtz, S., Seeger, M., & Ries, J. B. (2010). The rill experiment as a method to approach a quantification of rill erosion process activity. *Zeitschrift für Geomorphologie*, *54*, 47–64.

Wirtz, S., Seeger, M., & Ries, J. B. (2012). Field experiment for understanding and quantification of rill erosion processes. *Catena*, *91*, 21–34.

Wu, B., Wang, Z. L., Shen, N., & Wang, S. (2016). Modelling sediment transport capacity of rill flow for loess sediments on steep slopes. *Catena*, *147*, 453–462.

Xiao, H., Liu, G., Liu, P., Zheng, F., Zhang, J., & Hu, F. (2017). Sediment transport capacity of concentrated flows on steep loessial slope with erodible beds. *Scientific Reports*, *7*, 2350. https://doi.org/10.1038/s41598-017-02565-8

Xinlan, L., Longshan, Z., Jia, W., & Faqi, W. (2015). The effect of different soil erosion stages on surface roughness under simulated rainfall. *Nature Environment and Pollution Technology*, *14*, 9–16.

Yang, D. M., Fanga, N. F., & Shi, Z. H. (2020). Correction factor for rill flow velocity measured by the dye tracer method under varying rill morphologies and hydraulic characteristics. *Journal of Hydrology*, *591*, 125560. https://doi.org/10.1016/j.jhydrol.2020.125560

Zhang, G., Luo, R., Cao, Y., Shen, R., & Zhang, X. C. (2010). Correction factor to dye-measured flow velocity under varying water and sediment discharges. *Journal of Hydrology*, *389*, 205–213.

Zhang, G. H., Liu, Y. M., Han, Y. F., & Zhang, X. H. (2009). Sediment transport and soil detachment on steep slopes: I. transport capacity estimation. *Soil Science Society of America Journal*, *73*(4), 1291–1297.

Zhang, G., Wang, L., Tang, K., Luo, R., & Zhang, X. C. (2011). Effects of sediment size on transport capacity of overland flow on steep slopes. *Hydrological Sciences Journal*, *56*(7), 1289–1299.

Zhang, P., Tang, H., Yao, W., Zhang, N., & Xizhi, L. V. (2016). Experimental investigation of morphological characteristics of rill evolution on loess slope. *Catena*, *137*, 536–544.

**How to cite this article:** Di Stefano, C., Nicosia, A., Palmeri, V., Pampalone, V., & Ferro, V. (2021). Estimating flow resistance in steep slope rills. *Hydrological Processes*, *35*(7), e14296. https://doi.org/10.1002/hyp.14296